

Frustrated Square-Lattice Ferromagnets

Burkhard Schmidt, Nic Shannon¹, Karlo Penc², and Peter Thalmeier

The spin-1/2 Heisenberg antiferromagnet on a square lattice with additional next-nearest-neighbour interactions — commonly known as the J_1 - J_2 model — occupies a very special place in the literature of frustrated magnetism. Despite the apparent simplicity of its Hamiltonian

$$\mathcal{H} = J_1 \sum_{\langle ij \rangle_1} \vec{S}_i \cdot \vec{S}_j + J_2 \sum_{\langle ij \rangle_2} \vec{S}_i \cdot \vec{S}_k \quad (1)$$

where the sum labeled $\langle ij \rangle_1$ runs over nearest-neighbour and the sum $\langle ij \rangle_2$ is taken over diagonal next-nearest-neighbour bonds, this model with only one adjustable parameter (the ratio J_2/J_1) displays a great wealth of different physics.

For small $J_2/J_1 \ll 1$ its ground state is a simple (π, π) Néel antiferromagnet (AF) with reduced sublattice moment. For large $J_2/J_1 \gg 1$ it provides a paradigmatic example of “order from disorder” — a $(\pi, 0)$ collinear Néel phase (CAF) is selected by fluctuations from a degenerate manifold of classical ground states. For intermediate $J_2/J_1 \approx 0.5$, it exhibits a magnetically disordered “spin-liquid” phase, much studied as a potential realization of Anderson’s resonating valence bond (RVB) concept and a simple model for what happens on doping the layered AF La_2CuO_4 , the parent compound for a family of High- T_c superconductors [1].

Given the great theoretical interest in the J_1 - J_2 model, it is perhaps surprising that the first “ J_1 - J_2 compound”, $\text{Li}_2\text{VOSiO}_4$, was only discovered very recently [2]. $\text{Li}_2\text{VOSiO}_4$ has a layered structure, in which spin-1/2 V^{4+} ions reside within well-separated VO_4 pyramids, connected by SiO_4 tetrahedra to form a square lattice of magnetic sites. The exchange between V^{4+} ions is weak, indirect, and leads to both nearest-neighbour J_1 and next-nearest-neighbour J_2 interactions. In $\text{Li}_2\text{VOSiO}_4$ the ratio $J_2/J_1 \approx 10$, and the magnetic ground state is a $(\pi, 0)$ CAF [4]. However, this is only one point on the axis J_2/J_1 — are there more compounds which we can use to fill in the gaps?

The answer is yes, and the most recently discovered J_2/J_1 compounds $\text{Pb}_2\text{VO}(\text{PO}_4)_2$, $\text{BaZnVO}(\text{PO}_4)_2$ and $\text{SrZnVO}(\text{PO}_4)_2$ (described in “First Experimental Realization of a Frustrated Ferromagnetic

Square Lattice System”) turn out not only to have different ratios of J_2/J_1 , but to have ferromagnetic (FM) nearest-neighbour exchange J_1 . Given the complexity of the exchange path between neighbouring V^{4+} ions in these materials, FM J_1 interactions are not surprising in themselves. What is surprising is the extent of the literature devoted to the J_1 - J_2 model with FM J_1 at the time these compounds were discovered — one solitary paper [6]. The questions which we have chosen to address and which are described in this report, are the basic, fundamental properties of the J_1 - J_2 model with FM interactions:

- (i) What is the nature of its ground state as a function of J_2/J_1 ?
- (ii) What are the thermodynamic properties of each of these phases?

In the first part of this report we consider the phase diagram and low temperature properties of the J_1 - J_2 model, as summarized in Figure 1. In the second part we present comprehensive numerical results for its heat capacity $C_V(T)$ and magnetic susceptibility $\chi(T)$ in the high temperature para-

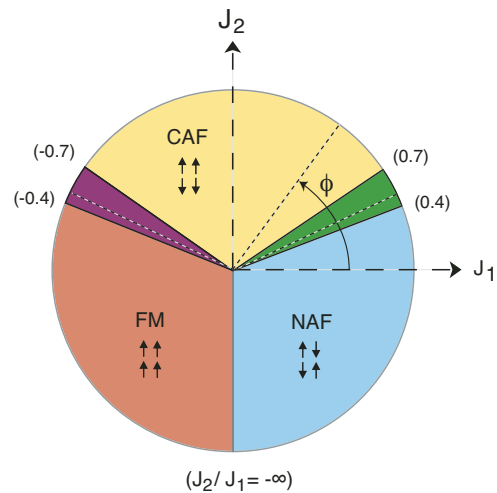


Fig. 1: Phase diagram for the spin-1/2 J_1 - J_2 Heisenberg model on a square lattice. Regions of simple (π, π) and collinear $(0, \pi)$ Néel order, and a simple FM phase are separated by two different spin liquid regions. The known spin liquid region for AF J_1 ($0.7 > J_2/J_1 > 0.4$) is a gapped, crystalline state. A new, gapless spin liquid region occurs for FM J_1 ($-0.7 < J_2/J_1 < -0.4$).

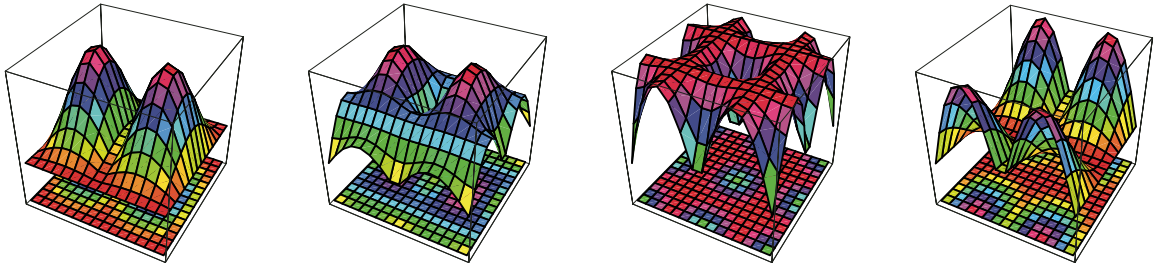


Fig. 2: Evolution of spinwave dispersion in CAF phase. From left to right - border with NAF, within CAF phase for AF couplings, pure next nearest neighbour exchange, border with FM. The horizontal plane shows the full Brillouin zone for the square lattice ($-\pi < q_x < \pi$; $-\pi < q_y < \pi$), the vertical axis the spin wave frequency $\omega(q_x, q_y)$.

magnetic phase. These can be compared directly to experiments and used to help determine exchange parameters in real materials.

Since the properties of the J_1 - J_2 model depend only on the ratio J_2/J_1 , and not the absolute size of the exchange coupling, it is convenient to introduce an overall energy scale $J_c = (J_1^2 + J_2^2)^{1/2}$ and a frustration angle ϕ such that $J_1 = J_c \cos(\phi)$, $J_2 = J_c \sin(\phi)$, and

$$\phi = \tan^{-1}(J_2/J_1). \quad (2)$$

Variation of the control parameter ϕ leads to quantum phase transitions between the ordered and spin-liquid like phases in Figure 1. As it turns out, fits to $C_V(T)$ and $\chi(T)$ at high temperatures frequently lead to two, equivalently good, values of $\phi = \phi_{\pm}$, and in the final part of the report we propose and make predictions for an experiment that can be used to distinguish between these values.

In the simplest approximation, the ground state of the J_1 - J_2 model is the classical state which minimizes the energy of Equation 1. In this approximation the model supports three distinct, collinear phases shown in Figure 1. A (π, π) Néel AF state (NAF) is found for antiferromagnetic $J_1 > 0$ and $J_2/J_1 < 0.5$, and a FM state for ferromagnetic $J_1 < 0$ and $J_2/|J_1| < 0.5$. For AF $J_2 > |J_1|/2$ the classical energy selects a manifold of states with nested NAF order parameters on the diagonal J_2 bonds. However, a collinear $(\pi, 0)$ Néel AF state (CAF) is selected by fluctuations [7].

Exactly on the lines $J_2/|J_1| = 0.5$ — shown by dashed lines in Figure 1 — there is not a single classical ground state, rather a whole family of commensurate and incommensurate spiral states. In this case fluctuations *do not* select a unique classical ground state, and this classical degeneracy has important consequences for the quantum phase diagram, discussed below.

We have performed semi-classical spin wave expansions for each of the three classical ordered phases of the J_1 - J_2 model. Typical results for the CAF phase are shown in Figure 2. At low temperatures, the thermodynamic properties of these phase are controlled by their spin wave excitations, and it is possible to calculate them explicitly within a semi-classical approximation — results for heat capacity and inverse magnetic susceptibility are shown in Figure 3 and Figure 4 (for further results, see [8]). However, at both edges of the CAF phase, the spin wave dispersion becomes ill-conditioned. It exhibits entire lines of zero modes, visible in Figure 2 for spectra calculated at $J_2 = |J_1|/2$, neighbouring the NAF and FM phases.

These zero modes lead to violent fluctuations about the CAF ordered state. Within the linear spin wave approximation, they lead to a divergence of the specific heat (Fig. 3), and are strong enough to destroy its ordered moment entirely (Fig. 5). This means that classical CAF order is no longer the right starting point to understand the ground state for $J_2/|J_1| \approx 0.5$.

The parameter range $J_2/J_1 \approx 0.5$ has been intensively studied for AF J_1 in the context of high temperature superconductivity. It is generally accepted that a new quantum “spin-liquid” phase forms bordering the NAF for $J_2/J_1 \approx 0.4$, in which spins form a “columnar-dimer” state — a crystal of singlets on parallel J_1 -bonds [9]. CAF order is not believed to be stable for $J_2/|J_1| \lesssim 0.7$. Our spin wave results provide a strong *prima facie* case to believe that another spin-liquid phase forms for FM J_1 , at the boundary between CAF and FM phases. More detailed numerical studies confirm this hypothesis, and reveal that this new spin-liquid is a gapless nematic state [10].

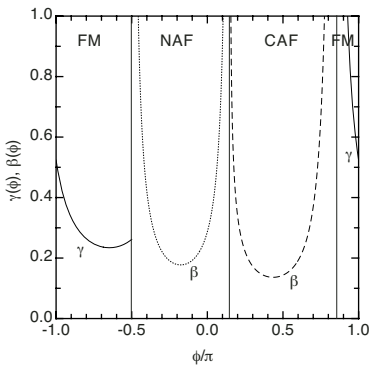


Fig. 3: Evolution of the heat capacity C_V as a function of the frustration angle ϕ . In FM regions the quantity plotted is the prefactor γ of $C_V = \gamma T$, and in AF regions the prefactor β of $C_V = \beta T^2$, where temperature is measured in units of J_c .

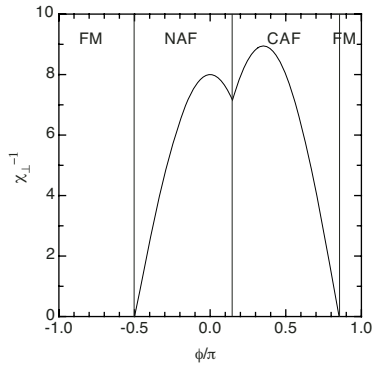


Fig. 4: Evolution of the inverse transverse susceptibility χ_{\perp}^{-1} as a function of the frustration angle ϕ , in units such that $J_c=1$ and $g\mu_B^2 = 1$.

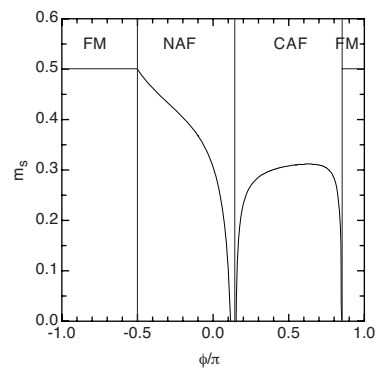


Fig. 5: Evolution of sublattice magnetization m_s as a function of the frustration angle ϕ within the three classical ordered phases of the J_1 - J_2 model (semi-classical spin wave approximation).

Further insight into the nature of the spin-liquid like phases at the margins of the collinear antiferromagnetic regime can be gained from our exact analytic diagonalization of the eight-site cluster. The resulting energy spectrum, classified by spin, is shown in Figure 6. The straight forward quantum phase transition between NAF and FM states for $\phi = -\pi/2$ appears as multiple crossings of ground state and excitation energy levels, all of which take place at the same critical value of $\phi = -\pi/2$.

At those values of ϕ at which the singlets associated with the NAF and CAF order parameters cross, the reordering of excited states *does not* take place at a single critical value of ϕ , but is spread over a finite range of ϕ . Simply counting where the lowest-lying triplet excitation crosses the lowest-lying singlet excitation on either side of the ground state crossing gives a remarkably good (if arbitrary) esti-

mate of the extent of the spin liquid region — from $J_2/J_1 = 0.38$ to $J_2/J_1 = 0.60$, values which are comparable with those found in the existing literature.

Examining the level crossings associated with the transition from CAF to FM we see the same extended structure. In this case applying the same naïve criterion based on the crossing of first excitations would predict a spin liquid region from $J_2/J_1 = -0.38$ to $J_2/J_1 = -0.60$.

In principle, the predictions for low temperature properties outlined above can be explored in great detail using elastic and inelastic neutron scattering. However, these techniques are expensive, time consuming, and require good single crystals of macroscopic dimension. It is much easier to characterize a new magnetic material using its high temperature heat capacity and susceptibility than to wait until large crystals become available for neu-

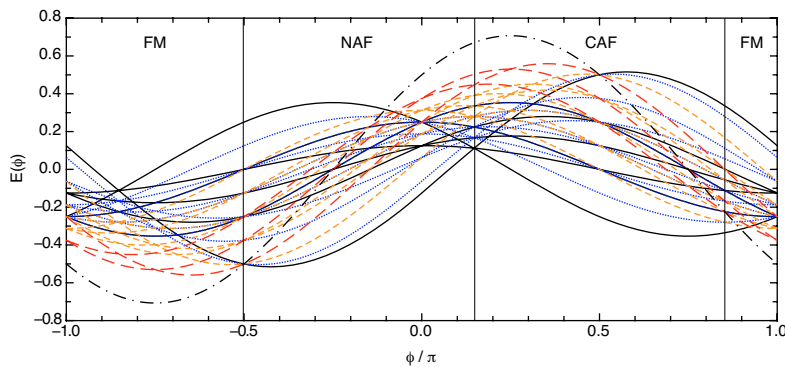


Fig. 6: Energy levels (per spin) of the 8 site cluster, classified according to total spin V as a function of the frustration angle f , in units of J_c : solid black lines — $\Omega = 0$ (singlet); dotted blue lines — $\Omega = 1$ (triplet); short-dashed orange lines — $\Omega = 2$; long-dashed red lines — $\Omega = 3$; dash-dotted black line — $\Omega = 4$ (maximal spin).

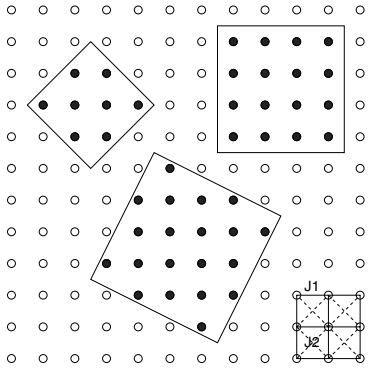


Fig. 7: Tiles of size eight, 16, and 20 used in the finite-temperature calculations. In the lower right corner, the labelling of the two exchange constants is illustrated.

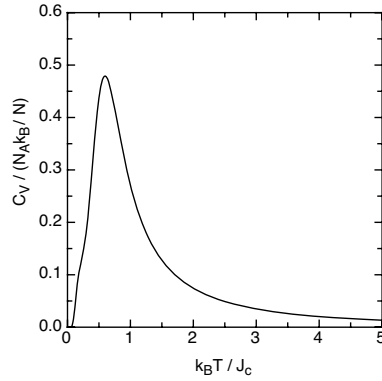


Fig. 8: Temperature dependence of the heat capacity $C_V(T)$ of the 20-site cluster for a frustration angle $\phi = 0.7\pi$.

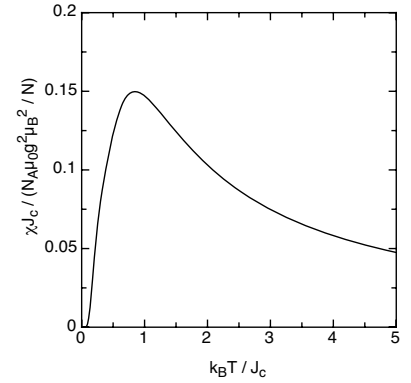


Fig. 9: Temperature dependence of the uniform magnetic susceptibility $\chi(T)$ of the 20-site cluster for a frustration angle $\phi = 0.7\pi$.

tron scattering. Fortunately, the quasi-2D vanadates which offer the best realization of the J_1 - J_2 model have exchange interactions (and therefore transition temperatures) of the order of a few Kelvin, such that “high temperatures” are in this case of the order of 10...100 K, easily achieved in a standard He cryostat.

In order to put measurements of heat capacity and magnetic susceptibility on a firm theoretical basis we also studied the thermodynamic properties of the J_1 - J_2 model in its high temperature paramagnetic phase [8]. These calculations have been accomplished through the analytic exact diagonalization of an 8-site cluster using a finite temperature Lanczos algorithm [11] to numerically calculate experimental response functions for clusters of $N = 16$ and $N = 20$ spins (Fig. 7).

Typical results are shown in Figure 8 (heat capacity) and Figure 9 (magnetic susceptibility), defined by

$$C_V(T) = \frac{N_A}{Nk_B} \frac{1}{T^2} \left(\langle H^2 \rangle - \langle H \rangle^2 \right) \quad (3)$$

$$\chi(T) = \frac{N_A \mu_0 g^2 \mu_B^2}{Nk_B} \frac{1}{T} \left(\langle (S_z^{\text{tot}})^2 \rangle - \langle S_z^{\text{tot}} \rangle^2 \right) \quad (4)$$

where $\langle \dots \rangle$ denotes the thermal average, $S_z^{\text{tot}} = \sum_i S_i^z$ the z component of the total momentum of the system, and N the number of sites of the system considered. N_A is the Avogadro constant, μ_0 the magnetic permeability, g the gyromagnetic ratio, μ_B the Bohr magneton, and k_B the Boltzmann constant. For the present nonmagnetic (zero field) case we have $\langle S_z^{\text{tot}} \rangle = 0$.

We have computed the heat capacity $C_V(T)$ in the full range of the frustration angle ϕ for different cluster sizes. Figure 10 shows the maximum of the heat capacity as a function of ϕ . The lower figure shows the frustration dependence of the temperature T_{C_V} at which the maximum is reached.

Two overall effects are clearly visible: (1) Apart from the regime with strong frustration, the maximum rises with increasing cluster size. (2) The maximum temperature decreases with increasing cluster size. Taken together, this indicates that entropy is shifted to lower temperatures, a sign of the missing long-range correlations not included in the partition function for the small clusters.

Our results are in qualitative agreement with those in [3,13]. They represent a quantitative improvement over the estimates of [3]. Direct comparison with [13] is made difficult by the ambiguities associated with analytic continuation of a series using Padé approximants, and by the fact that the limited number of cluster sizes, we can use at present, do not permit a finite size scaling analysis. In agreement with [3], C_V^{max} drops sharply near the crossover between the spin liquid regime and the collinear phase around $J_2/J_1 \approx 0.6$, corresponding to $\phi/\pi \approx 0.17$. Similar drops occur at the borders of the FM regime with the NAF and CAF phases, respectively. These drops are accompanied by a smaller T_{C_V} in order to conserve the entropy of the system.

In Figure 11, the behaviour of the maximum of the magnetic susceptibility χ^{max} together with the temperature at which the maximum is reached is

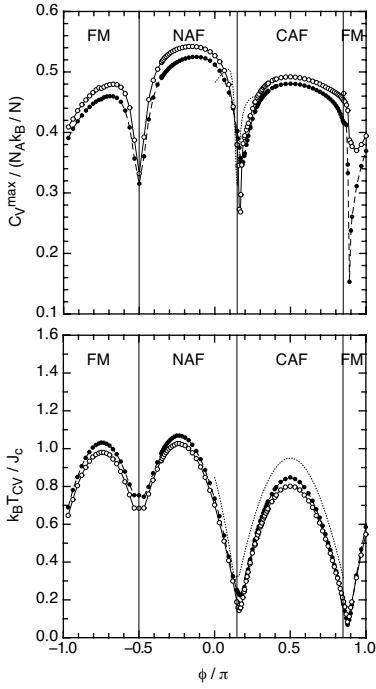


Fig. 10: Maximum of the heat capacity $C_V(T)$ and its position T_{C_V} as functions of the frustration angle ϕ . The open (solid) circles denote the results for the 20-site (16-site) cluster, the dotted line denotes the eight-site cluster.

displayed. In contrast to the heat capacity, $\chi(T)$ does not display an anomaly upon crossing the spin-liquid regime. The maximum value diverges near the crossover to the FM regime, while its position approaches $T = 0$, which is the expected behavior. Apart from that, the parameter dependence of the maximum position T_χ is qualitatively the same as for T_{C_V} .

Our predictions for the maximum values of $C_V(T)$ and $\chi_V(T)$, and the temperatures at which they occur can be compared directly with experimental data for square lattice vanadates (Table 1). However carefully these fits are constrained, they always give two possible values for the frustration parameter ϕ [13]. In the case of $\text{Pb}_2\text{VO}(\text{PO}_4)_2$, one of these fits corresponds to FM J_1 and a CAF ground state, the other to AF J_1 and a NAF ground state. To distinguish between the two possibilities ϕ_\pm , further diagnostic tools are necessary. The sign and magnitude of J_1 could easily be resolved by performing inelastic neutrons scattering on large single crystals of $\text{Pb}_2\text{VO}(\text{PO}_4)_2$, however at present, only powder samples and very small single crystals are available.

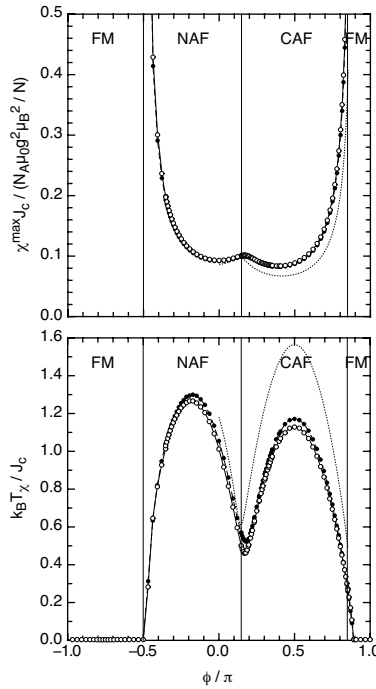


Fig. 11: Maximum of the uniform magnetic susceptibility $\chi(T)$ and its position T_χ as functions of the frustration angle ϕ . The open (solid) circles denote the results for the 20-site (16-site) cluster, the dotted line denotes the eight-site cluster.

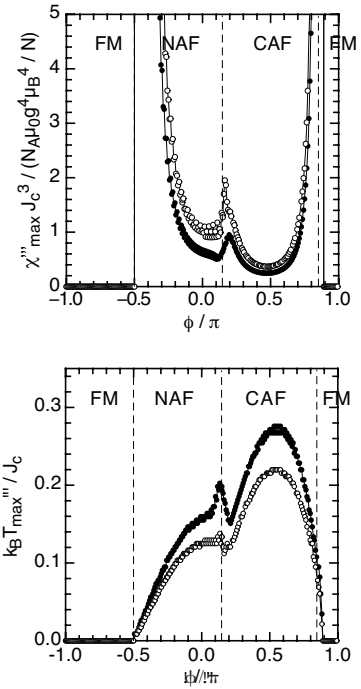


Fig. 12: Maximum value (top) and maximum temperature (bottom) of the third-order magnetic susceptibility of the frustrated Heisenberg antiferromagnet. The filled dots represent the exact-diagonalization results for a 16-site cluster, the open circles correspond to a 20-site cluster.

Therefore, we have developed two alternative approaches to determine ϕ .

The first is the measurement of the *third-order susceptibility*, defined via the small-field expansion of the magnetisation $M(T)$:

$$M = \chi \cdot B + \frac{1}{3!} \chi''' \cdot B^3 + \dots, \quad (5)$$

$$\chi''' = \frac{N_A \mu_0 (g \mu_B)^4}{N k_B^3} \frac{1}{T^3} \left(\langle (S_{\text{tot}}^z)^4 \rangle - 3 \langle (S_{\text{tot}}^z)^2 \rangle^2 \right) \quad (6)$$

where the symbol $\langle \dots \rangle$ denotes the trace over the statistical operator for zero magnetic field B . χ''' takes on different values in the CAF and NAF phases [14]:

In all non-ferromagnetic phases of the model, the temperature dependence of $\chi'''(T)$ has a pronounced maximum at a temperature T_{max}''' , vanishes at a temperature T_0''' , passes through a tiny minimum at a temperature T_{min}''' , and eventually approaches the high-temperature T^{-3} dependence. We have followed these characteristic temperatures as a function of the frustration angle. The initial maximum temperature, together with the value of χ''' at that point, are shown for the 16-site (solid

	Pb ₂ VO(PO ₄) ₂		Li ₂ VOSiO ₄				Li ₂ VOGeO ₄			
	[5]		[2]	[3]	[12]	[13]	[2]	[12]		
Θ_{CW} [K]	4		7.4	8.2	9.65	7.2	5.2	9.8		
Θ_{CW}/T_χ	0.49		1.39	1.69			1.49			
ϕ/π	0.67	0.64	0.41	0.27	0.47	0.43	0.36	0.38	0.43	0.33
ϕ_\pm/π		-0.11	0.03	0.13			0.06	0.08	0.07	
$(J_1, J_2)_-$	-1.64	-2.13	3.5	1.1	11.7	4.76	2.13	2.5	4.76	1.69
$(J_1, J_2)_+$		-0.37	0.1	0.44			0.18	0.25	0.24	

Tab. 1: Compilation of the experimental results and theoretical estimates on the Curie-Weiss temperature $\Theta_{CW} = (J_1 + J_2)/k_B$, the ratio Θ_{CW}/T_ϕ of it to the maximum position of the uniform magnetic susceptibility $\chi(T)$ and the corresponding frustration parameters. The experimental data are taken from [2,3,5]. The displayed theoretical values for the frustration parameters obtained by fits to high-temperature series expansions are taken from [12,13]. The reference numbers are used to label the corresponding columns. The unlabelled columns contain our own estimates derived from the dependence of Θ_{CW}/T_ϕ on ϕ . The \pm subscripts of ϕ and J_2/J_1 distinguish the two different possible points in the (J_1, J_2) phase diagram.

dots) and 20-site cluster (open circles) in Figure 12. The maxima occur at temperatures $T_{\max} \ll J_c$, therefore finite-size effects are large.

The characteristic temperatures, together with the values of χ''' at maximum and minimum, are compiled in Table 2 for $\phi = -0.11\pi$ and 0.64π . Likewise shown is the ratio Θ_{CW}/T_{\max} of the Curie-Weiss temperature to the position of the characteristic maximum of the linear susceptibility $\chi(T)$ taken from Ref. [8], which is equal for both values $\phi = \phi_\pm$. Together with the results from Ref. [8], our findings should be useful in determining the precise value of ϕ for a given J_1 - J_2 compound, as exemplified here for Pb₂VO(PO₄)₂. The second approach is to use diffuse neutron scattering, which is effective for powder samples and in the paramagnetic phase — to measure the angle-integrated spin structure factor $S(\mathbf{q}, T)$.

$S(\mathbf{q}, T)$ contains information about fluctuations of magnetic order for $T > T_c$, and has quite different properties for values of ϕ corresponding to FM and

$\frac{\phi}{\pi}$	$\frac{\Theta_{CW}}{T_{\max}}$	$\frac{k_B T_{\max}'''}{J_c}$	$\frac{k_B T_0'''}{J_c}$	$\frac{k_B T_{\min}'''}{J_c}$	$\frac{\chi_{\max}''' J_c^3 N}{N_A \mu_0 g^4 \mu_B^4}$	$\frac{\chi_{\min}''' J_c^3 N}{N_A \mu_0 g^4 \mu_B^4}$
-0.11	0.49	0.11	1.69	2.37	1.41	-0.0018
0.64	0.49	0.21	1.45	2.02	0.64	-0.0029

Tab. 2: Characteristic values for the third-order susceptibility obtained for the two different frustration angles $\phi = -0.11\pi$ and $\phi = 0.64\pi$ which are equally possible for the compound Pb₂VO(PO₄)₂. The second column lists the ratio of the Curie-Weiss temperature to the maximum temperature of the linear susceptibility as obtained from Ref. [8].

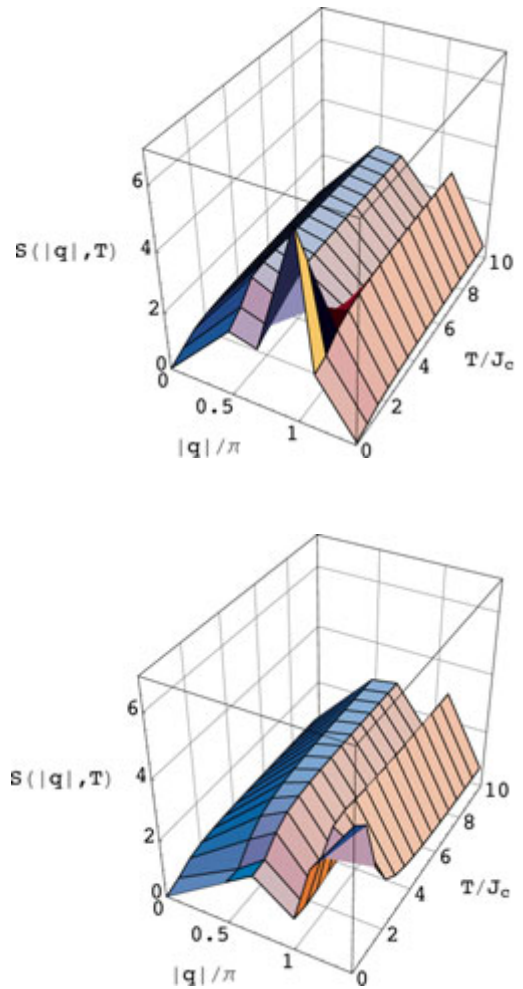


Fig. 13: Static spin structure factor $S(\mathbf{q}, T)$ of the 16-site cluster for $J_1/k_B = -6$ K, $J_2/k_B = 10$ K (collinear phase, top) and $J_1/k_B = 10$ K, $J_2/k_B = -6$ K (Néel phase, bottom figure). The values chosen for J_1 and J_2 correspond to those given for Pb₂VO(PO₄)₂ in [5].

AF J_1 — where FM J_1 favors a CAF ground state, $S(\mathbf{q}, T)$ is strongly peaked for $|\mathbf{q}| \sim \pi$, while where AF J_1 favors a NAF ground state, $S(\mathbf{q}, T)$ is strongly peaked for $|\mathbf{q}| \sim \phi 2\pi$. Moreover, the explicit temperature dependence of $S(\mathbf{q}, T)$ contains information about the absolute values of J_1 and J_2 .

Examples of predictions for $S(\mathbf{q}, T)$ taken from our finite temperature Lanczos calculations are given in Figure 13. We have chosen the two frustration angles $\phi_- = 0.64$ where the system is in the collinear phase and $\phi_+ = -0.11$ corresponding to the Néel phase. These values are, again, those determined from the static susceptibility of $\text{Pb}_2\text{VO}(\text{PO}_4)_2$. For the collinear phase, the maximum of $S(\mathbf{q}, T)$ is located at $|\mathbf{q}| = \pi$, in the Néel phase $S(\mathbf{q}, T)$ reaches its maximum near the zone boundary where $|\mathbf{q}| = \sqrt{2}\pi$.

Very recent diffuse neutron scattering measurements of powder samples of $\text{Pb}_2\text{VO}(\text{PO}_4)_2$ [15] show unambiguously that $S(\mathbf{q}, T)$ is peaked for $|\mathbf{q}| \sim \pi$, and has a temperature dependence compatible with fits to $\chi(T)$ and $C_V(T)$ for FM J_1 . These experiments, taken together with our calculations provide definitive proof that $\text{Pb}_2\text{VO}(\text{PO}_4)_2$ does indeed have FM J_1 interactions. This means that $\phi_+/\pi \approx 0.64$ is the proper frustration angle leading to $J_1 \approx -5$ K, $J_2 \approx 10$ K for this compound.

The study of two-dimensional frustrated ferromagnets is very much in its infancy. However, there is every reason to believe that these systems will prove as interesting as the widely studied two-dimensional frustrated antiferromagnets. Indeed frustrated ferromagnets have already delivered a number of big surprises — notably the spin liquids observed in He III absorbed on graphoite [16], and in the new quasi-two dimensional oxychloride cuprate $(\text{CuCl})\text{LaNb}_2\text{O}_7$ [17]. If, as seems overwhelmingly probable, $\text{BaZnVO}(\text{PO}_4)_2$ and $\text{SrZnVO}(\text{PO}_4)_2$ also have FM J_1 , then an entire family of FM J_1 - J_2 compounds is now available to study, each member with its own characteristic level of frustration.

The work reported here provides a solid theoretical foundation for further studies of frustrated

square lattice FM's such as $\text{Pb}_2\text{VO}(\text{PO}_4)_2$. However there are many more interesting questions which one could hope to answer. For example, what are the different phases of these systems under applied magnetic field, where frustrated AF's are known to exhibit new metamagnetic states? Is it possible, by judicious chemical substitutions to tune the exchange interactions of a square lattice vanadate into the proposed spin-liquid region? Can the suppression of T_c by competing interactions in frustrated ferromagnets shed any light on the nature of quantum critical points in itinerant magnets? It is our hope that all of these questions will be addressed in the future.

References

- [1] For a review, see e.g. *G. Misguich and C. Lhuillier*, in "Frustrated spin systems", edited by H.T. Diep, World-Scientific (2004).
- [2] *R. Melzi et al.*, Phys. Rev. Lett. **85** (2000) 1318.
- [3] *R. Melzi et al.*, Phys. Rev. B **64** (2001) 024409.
- [4] *A. Bombardi et al.*, Phys. Rev. Lett. **93** (2004) 027202.
- [5] *E. Kaul et al.*, J. Magn. Magn. Mat. **272-276(II)** (2004) 922.
- [6] *D. V. Dmitriev et al.*, Phys. Rev. B **55** (1997) 3620.
- [7] *E. F. Shender*, Sov. Phys. JETP **56** (1982) 178.
- [8] *N. Shannon, B. Schmidt, K. Penc and P. Thalmeier*, Eur. Phys. J. B **38** (2004) 599.
- [9] *P. Sindzingre*, Phys. Rev. B **69** (2004) 094418, and reference therein.
- [10] *N. Shannon, T. Momoi and P. Sindzingre*, Phys. Rev. Lett. **96** [2006] 027213.
- [11] *J. Jaklic and P. Prelovsek*, Adv. Phys. **49** (2000) 1.
- [12] *H. Rosner et al.*, Phys. Rev. Lett. **67** (2003) 014416.
- [13] *G. Misguich et al.*, Phys. Rev. B **68** (2003) 113409.
- [14] *B. Schmidt and P. Thalmeier*, Physica B **359-361** (2005) 1387.
- [15] *M. Skoulatos et al.*, in preparation.
- [16] *K. Ishida et al.*, Phys. Rev. Lett. **79** (1997) 3451.
- [17] *H. Kageyama et al.*, J. Phys. Soc. Jpn. **74** (2005)1702.

¹ Present address: University of Bristol, Bristol, United Kingdom

² Research Institute of Solid State Physics and Optics, Budapest, Hungary